






Kinematic properties and ages of extended fast, neutral gas around η Carinae: tracing the pre-eruption bipolar wind

Jon A. Morse ^{1,2}  and Nathan Smith ³

¹*BoldlyGo Institute, 31 West 34th Street, Floor 7 Suite 7159, New York, NY 10001, USA*

²*Division of Physics, Mathematics and Astronomy, California Institute of Technology, Pasadena, CA 91106, USA*

³*Steward Observatory, University of Arizona, 933 North Cherry Avenue, Tucson, AZ 85721, USA*

Accepted 2023 December 7. in original form 2023 November 6

ABSTRACT

We present proper-motion measurements and long-slit spectroscopy of the Mg II nebula around η Carinae obtained with the Wide Field Camera 3 and Space Telescope Imaging Spectrograph (STIS) aboard the *Hubble Space Telescope*. Detailed kinematics of the Mg II-emitting material constrain the geometry and history of mass-loss from η Car, and provide estimated ejection dates, assuming linear, ballistic motions. These measurements show that the neutral gas immediately outside the Homunculus – i.e. material into which the Homunculus is now expanding – was expelled over several decades prior to the Great Eruption, thus representing unshocked pre-eruption stellar wind. Material outside the Homunculus is therefore not part of a Hubble-like flow from the Great Eruption itself. This result discriminates between versions of merger-in-a-triple models for η Car. The STIS spectrum of Mg II-emitting gas along the projected outflow axis displays radial velocities consistent with bipolar expansion, redshifted several hundred km s⁻¹ towards the northwest, similarly blueshifted towards the southeast, and with low internal velocity dispersion. The η Car system was therefore losing mass in a relatively fast, low-density polar wind for several decades that probably traces the critical inspiral phase preceding a merger event.

Key words: circumstellar matter – stars: evolution – stars: winds, outflows.

1 INTRODUCTION

There are many examples where the end phases of massive star evolution involve prodigious mass-loss, but the mechanisms and triggers of this mass-loss remain uncertain. Connecting distinct stellar end states to the observed diversity of supernovae (SNe) is particularly murky for the highest mass stars. The late evolutionary phases of very massive stars are punctuated by bursts of episodic mass-loss that are comparable to or even more important than steady winds (Smith & Owocki 2006), exemplified by luminous blue variables (LBVs). These eruptions may dominate mass-loss in the most massive stars, but despite their importance, the physical trigger, mechanism, time-scales/duty cycle, and energy source are not well constrained (see Smith 2014 for a review).

A common hypothesis for LBV eruptions is that mass-loss is driven by super-Eddington winds (Shaviv 1998; Owocki et al. 2004; Smith & Owocki 2006; Quataert et al. 2016), but an unambiguous source of the extra luminosity or what triggers its sudden release, including the possible role of a binary companion, is not well understood. Recent studies have shown, however, that in some cases

the energy budget causes severe problems for a super-Eddington wind, and observations seem to indicate a more explosive (i.e. hydrodynamic) mechanism (Smith et al. 2003a, 2018b, c; Smith 2008, 2013). Like core-collapse SNe and their progenitor stars, it is important to understand the physical state of LBVs like η Carinae in the years just before they erupt, as well as the eruptions themselves.

The massive star η Carinae is our most valuable source of information about LBV giant eruptions, due to its proximity and its historical ‘Great Eruption’ observed in the 1840s. It is among the most luminous stars in the Milky Way and has displayed extreme instability (Davidson & Humphreys 1997). Three key observables make η Car uniquely valuable: (1) There is a detailed light curve of the 19th century Great Eruption (Smith & Frew 2011), constraining the timing and radiative energy budget of the event. (2) Light echoes from this eruption allow one to recover spectra of the historical event (Rest et al. 2012; Prieto et al. 2014; Smith et al. 2018b, c), which can now be compared directly with spectra of extragalactic transients and SN precursors. (3) Eruptions have created the beautifully complex nebula surrounding η Car, the inner portion of which is called the ‘Homunculus’ (Gaviola 1950; Morse et al. 1998). Proper motions measured using *Hubble Space Telescope* (HST) and historical ground-based imagery have verified that the Homunculus is the main product of the 1840s eruption (Currie et al. 1996; Smith & Gehrz 1998; Morse et al. 2001; Smith 2017), and studies of chemical abundances reveal N-enriched material (Davidson et al. 1986; Smith & Morse 2004) indicating that it is CNO processed stellar ejecta.

* E-mail: jamorse@boldlygo.net

† Visiting Associate in Astronomy.

‡ Present address: AstronetX PBC, 55 Post Road West, FL 2 STE 239B, Westport, CT 06880, USA.

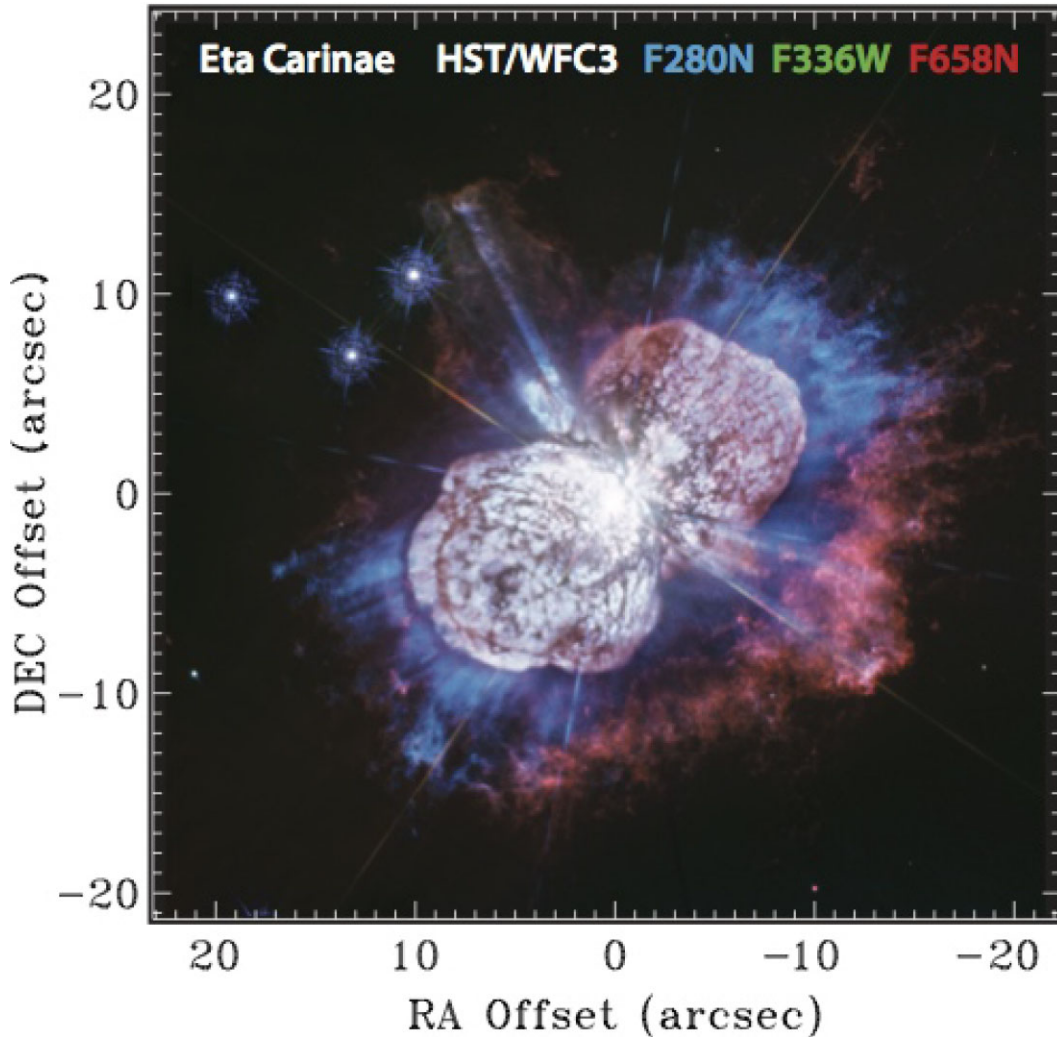


Figure 1. Colour *HST*/WFC3 image of η Car from Paper I with *F280N* (Mg II) in blue, *F336W* (blue continuum) in green, and *F658N* ([N II] + redshifted $H\alpha$) in red.

Even farther outside the Homunculus, η Car is surrounded by a ragged spray of clumpy material, known as the ‘Outer Ejecta’, displaying very bright [N II] emission (Thackeray 1950; Walborn 1976; Walborn, Blanco & Thackeray 1978; Walborn & Blanco 1988; Davidson et al. 1986; Leutenegger, Kahn & Ramsay 2003; Smith & Morse 2004). The structure and kinematics of η Carinae’s Outer Ejecta have been analysed by Kiminki, Reiter & Smith (2016) through proper motions measured using *HST* emission-line images (mostly tracing $H\alpha$ and [N II] emission; see also Morse et al. 2001), and by Mehner et al. (2016) with Very Large Telescope Multi Unit Spectroscopic Explorer spatially resolved radial velocities. Proper motions of these Outer Ejecta have shown that they originated from at least two major mass ejection episodes in the 13th and 16th centuries, plus some material closer to the Homunculus that may have been ejected during or shortly before the 19th century Great Eruption (Kiminki, Reiter & Smith 2016). These various ejection episodes had an asymmetric geometry that was different in each epoch (Kiminki, Reiter & Smith 2016; Mehner et al. 2016). In contrast, the axisymmetric Homunculus has a single, well-determined ejection date of 1847 (Morse et al. 2001; Smith 2017).

Smith & Morse (2019, hereafter Paper I) presented an *HST* ultraviolet (UV) image of Mg II $\lambda\lambda 2800$ emission in the nebula

around η Carinae using the *F280N* filter on the Wide Field Camera 3 (WFC3). The image revealed strong Mg II emission, but with unexpected morphology. The Mg II is generally anticorrelated with other line emission features seen in typical tracers like $H\alpha$, [N II], or [Fe II] emission (see Fig. 1). Mg II emission provides an entirely new view of η Car, revealing additional ejecta mass and kinetic energy outside the main bipolar Homunculus that has been invisible in all other imaging filters used so far. Paper I concluded that most of the Mg II emission is due to resonance scattering of near-UV starlight by warm, freely expanding (unshocked) material, where H is mostly neutral. (Some Mg II features truncate at shocked gas knots where [N II] and $H\alpha$ emission is also observed.) There are even dark radial streaks in the Mg II nebula outside the approaching lobe that are best explained as projected shadows (i.e. sunbeams or God rays) from dust features on the surface of the lobe. Since this Mg II emission lies immediately outside the main bipolar Homunculus nebula created by the Great Eruption, it may hold critical clues about the acceleration of the ejecta and the mass-loss and instability of the star in the decades leading up to the Great Eruption that cannot be ascertained any other way.

Based on outflow velocities seen in light echo spectroscopy, combined with many other observational clues, Smith et al. (2018b)

proposed a model for η Car wherein the Great Eruption resulted from a merger in a triple system, leaving behind the eccentric binary system and bipolar nebula we see today. Hirai et al. (2021) presented numerical simulations for portions of this merger scenario, and suggested a somewhat different explanation for the origin of the bipolar shape of the Homunculus. The kinematic age of the material in the Mg II nebula offers a direct test of these two scenarios, as we discuss below.

This paper presents the first kinematic measurements of the Mg II filaments discovered in Paper I that lie just outside of the main lobes of the Homunculus nebula, but interior to the N-rich Outer Ejecta. Section 2 summarizes the new *HST* images and spectra, Section 3 presents the Mg II proper-motion measurements from the two image epochs, and Section 4 presents the kinematics from the long-slit spectrum. The interpretation of these results is discussed in Section 5, and then a summary of our results is found in Section 6.

2 OBSERVATIONS

Fig. 1 reproduces the colour image of η Car from Paper I using data obtained through the *HST* WFC3 *F280N* (blue), *F336W* (green), and *F658N* (red) filters. The blueish nebulosity reveals Mg II emission from gas in the space between the dusty lobes of the Homunculus and the shock-excited outer debris field (in red). This *HST F280N* image, obtained as part of programme ID GO-15289, occurred on 2018 March 5, and forms the first epoch for our Mg II proper-motion measurements. The second epoch was acquired as part of programme ID GO-15823 on 2020 February 12. Both image sets were reduced and calibrated on the fly during extraction from the Mikulski Archive for Space Telescopes (*MAST*) at the Space Telescope Science Institute (STScI). Paper I describes the data reduction procedure for the 2018 *F280N* image. For the purpose of measuring proper motions of the extended nebulosity, we likewise followed the data handling procedures described in Paper I, and then used 68 stars as tie points in the field surrounding η Car to align the 2018 and 2020 images. While the stars in the surrounding Tr16 cluster are moving, their typical velocities of $\lesssim 10$ km s⁻¹ (Kiminki & Smith 2018) are much smaller than the measured motion of Mg II-emitting features. The rms residuals in the quadratic X , Y fits were ~ 5 mas, corresponding to < 10 per cent of the magnitude of the motions being measured in the outer Mg II nebulosity. Details of the proper motions are shown in Fig. 2, and we discuss the proper motion results in Section 3.

Long-slit spectra with the *HST* Space Telescope Imaging Spectrograph (STIS) were also obtained at two position angles (PAs) as part of programme ID GO-15823. The observations employed the G230MB grating, which provided a spectral dispersion of 0.15 Å pixel⁻¹ (~ 16 km s⁻¹ pixel⁻¹) and 156 Å total wavelength coverage centred at 2794 Å. The long slit covered 52 arcsecs in the cross-dispersion direction, extending beyond the Mg II nebulosity detected in the WFC3 *F280N* images, with an image scale of ~ 0.05 arcsec pixel⁻¹. The first spectrum from 2020 May 30 at PA $\sim 50^\circ$ cut across the Homunculus just north of the central star, and included the NN and S Condensations, using the nomenclature of Walborn, Blanco & Thackeray (1978). Unfortunately, this spectrum did not detect significant extended Mg II emission through the STIS 52×0.2 slit. We therefore used the wider 52×0.5 slit for the second spectrum at PA 313.4° (roughly parallel to the Homunculus polar axis) on 2021 February 27, placing it west of the central star and including outer Mg II filaments just beyond the edges of both lobes of the Homunculus. The central region around the Mg II doublet in the processed 2D long-slit spectrum and resulting extracted 1D spectra of extended Mg II emission are shown in Fig. 3. The kinematic

measurements are further discussed in Section 4. Observations used in this study are summarized in Table 1.

3 PROPER MOTIONS IN WFC3 F280N IMAGES

We employed software used in previous studies (see Morse et al. 2001; Kiminki, Reiter & Smith 2016) to measure proper motions in the Homunculus and outer Mg II nebula of η Car using the two *HST*/WFC3 *F280N* images. A small region (box) isolating a nebular feature in the first epoch image is raster scanned over a somewhat larger region in the second epoch image to generate a correlation peak using a difference-squared cross-correlation algorithm described by Currie et al. (1996). The position of the peak is measured to a fraction of a pixel and indicates the speed and direction of the transverse motion of the feature, which is converted to km s⁻¹ knowing the time between observations and assuming a distance to the target ($D = 2.3$ kpc for η Car; e.g. Smith 2006b; Shull, Darling & Danforth 2021). The top panel of Fig. 2 shows the first-epoch 2018 *F280N* image with an assortment of boxes superposed on the southeast (SE) and northwest (NW) lobes of the Homunculus and outer Mg II nebula. The boxes were chosen to isolate specific features that could be followed by the measurement code, while avoiding artefacts in the images such as the diffraction spikes from the central star.

The lower panel of Fig. 2 plots the proper-motion measurements. Regions on the lobes of the Homunculus were measured as a check that the image alignment and measurement process independently reproduced the results obtained from prior studies using different filter bandpasses (e.g. Morse et al. 2001; Smith 2017). The points in the plot corresponding to regions in the SE and NW lobes have low scatter along a linear (Hubble-law) trajectory, coinciding well with the dashed line for an 1847 ejection date that is overplotted (i.e. not a fit to the points).

The results for features in the Mg II nebula differ markedly from the measurements in the lobes. The nebular points generally trend linearly, but jump to lower velocity at ~ 11 arcsec projected distance from the star beyond the edge of the lobes. The corresponding ejection dates range over several decades prior to the Great Eruption. The nebular features being tracked are generally larger scale and more diffuse than features on the surface of the lobes. Hence, with the limited time baseline of only 2 yr between epochs, measurements of the expansion of the lobes show smaller intrinsic measurement uncertainties and scatter in Fig. 2 than the puffier Mg II filaments. Future observations that provide a longer time baseline between epochs – such that the features move a distance corresponding to a substantial fraction of their projected size – will enable more precise measurements of the outer Mg II filaments. Nevertheless, as discussed below, these results definitively show that the outer Mg II nebula has a different age than the Homunculus, and appears to comprise wind material ejected over several decades prior to the Great Eruption.

4 STIS SPECTROSCOPY

The velocity field near the central star and across the lobes of the Homunculus is very complex (e.g. Smith et al. 2003a). The Mg II $\lambda\lambda 2796, 2803$ doublet lines display a mixture of emission and absorption features including reflected stellar wind components, *in situ* absorption and emission, and rest velocity interstellar absorption. We describe several of these components in the caption to Fig. 3, but our purpose with the new deeper STIS spectra was to detect and characterize the extended Mg II nebulosity that is found $\gtrsim 10$ arcsec from the star along the slit. The redshifted (NW) and blueshifted (SE) nebular emission is highlighted by the brackets in the lower

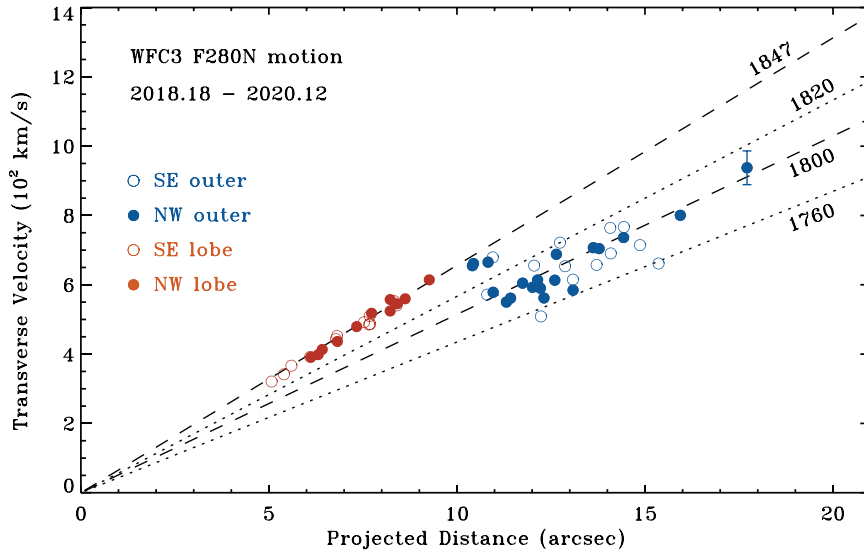
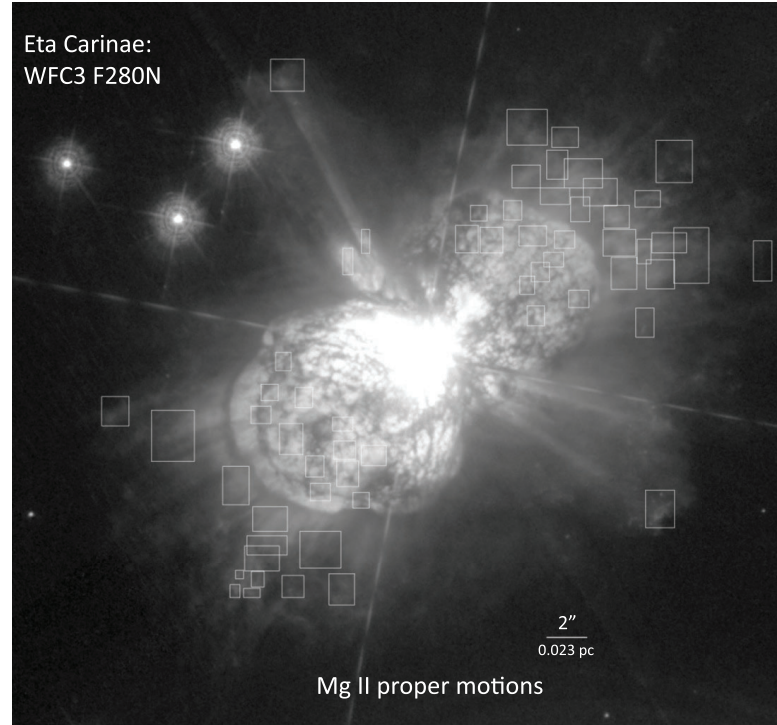


Figure 2. *Top panel:* Boxes projected on the 2018 WFC3 F280N image used to isolate different emission features in the η Car Homunculus and surrounding nebula for measuring proper motions. *Bottom panel:* Proper-motion measurements converted to transverse velocity assuming $D = 2.3$ kpc, as a function of projected radial distance from the central star. Red symbols correspond to marked features in the polar lobes and blue symbols correspond to boxes for marked features in the Mg II nebula outside the Homunculus. Unfilled symbols are for features to the SE of the star, and filled are towards the NW. The diagonal lines show proper-motion trends for a few representative ejection dates, assuming linear motion.

panel of Fig. 3 and drawn as light-blue swaths in the top panel. There are slight wiggles and gradients in the 2D profiles but essentially the emission captured shows fairly constant radial velocities in the cross-dispersion direction – i.e. roughly radially from the star beyond the edges of the lobes. In general, the $\lambda 2796$ line of the doublet appears consistently weaker than the $\lambda 2803$ line, as though suffering variable but significant absorption all along the slit due to the overlapping kinematic components. (There is also the unfortunate presence of an STIS repeller wire shadow covering the middle of the extended NW Mg II emission.)

The insets in the lower panel of Fig. 3 show intensity tracings of the spectrum at the positions of the outer Mg II nebula. These tracings overplot simple Gaussian curves fit to the emission components, where we initially fit the stronger 2803 \AA line at both positions, and then forced the weaker 2796 \AA line to be shifted by -768 km s^{-1} relative to Mg II $\lambda 2803$, with the same full width at half-maximum (FWHM) as the stronger line. We find that to the SE, the Mg II emission is blueshifted by $-340 (\pm 10) \text{ km s}^{-1}$ and the $\lambda 2796/\lambda 2803$ intensity ratio is 0.3 ± 0.02 . In the NW portion of the Mg II nebula, the centroid of the emission is at $+340 (\pm 10)$

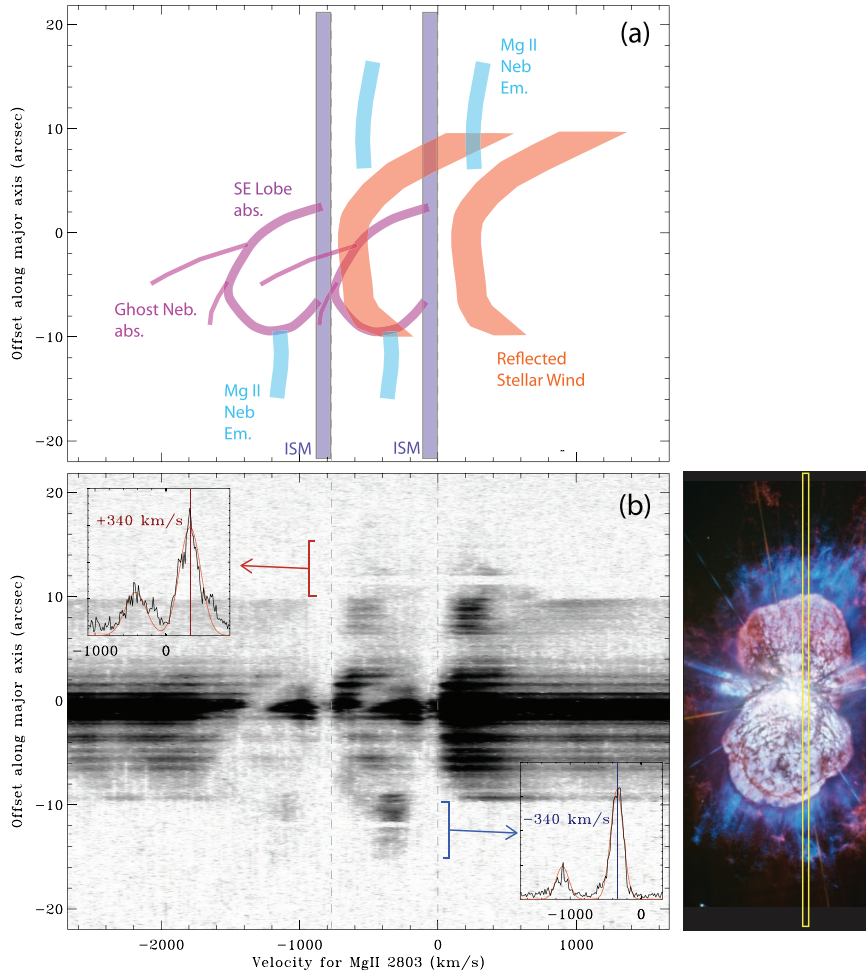


Figure 3. Kinematic structures in the long-slit STIS spectra. (a) Various emission and absorption structures of the Mg II doublet are traced and noted, including ISM absorption features (purple), blueshifted absorption structures in the SE polar lobe and ‘Ghost Nebula’ (magenta; Currie, Dorland & Kaufer 2002; Smith 2002), broad redshifted emission that is reflected Mg II emission from η Car’s stellar wind (orange), and the resonant scattered Mg II emission from the outer nebulosity to the NW and SE (blue). The position along the Y-axis in this plot corresponds to position angle 313.4° . (b) Grey-scale 2D image of the long-slit STIS spectrum of the Mg II doublet structure, with the velocities on the X-axis corresponding to the $\lambda 2803$ line. The vertical dashed grey lines show zero velocity for each of the two lines. The two insets in the upper-left and lower-right show intensity tracings of the outer Mg II nebulosity with Gaussian fits to the line profiles. These indicate Doppler shifts of $\pm 340 \text{ km s}^{-1}$. The colour image at the lower-right shows the STIS 52×0.5 slit position across the Homunculus and Mg II nebula.

Table 1. HST Mg II observations used in this study.^a

UT date	Instrument	Spectral element	$\lambda_{\text{cen}}/\text{width}$ (\AA)	Total exposure (s)
5 Mar 2018	WFC3/UVIS	F280N	2798/43	3930
12 Feb 2020	WFC3/UVIS	F280N	2798/43	5288
27 Feb 2021	STIS/NUV	G230MB + 52×0.5 slit	2794/156	9400

^aObservations acquired as part of programme IDs GO-15289 and GO-15823.

km s^{-1} and the $\lambda 2796/\lambda 2803$ intensity ratio is 0.4 ± 0.04 . The FWHM line widths in both the northern and southern nebula are $\sim 200 \text{ km s}^{-1}$, larger than the intrinsic spectral resolution as indicated by the narrow, rest velocity Mg II $\lambda 2796$, 2803 absorption lines in the 2D spectrum. This line width is not thermally driven and so must reflect the dispersion caused by the viewing geometry and/or (sub-sonic) mechanical turbulence in the neutral wind.

Interpretation of the observed flux ratio of the two lines in the Mg II doublet is complicated. Under normal circumstances, an atomic

gas cloud that is optically thin as it resonantly scatters Mg II will produce stronger flux in the 2796 \AA line, with a $\lambda 2796/\lambda 2803$ flux ratio of roughly 1.5 to 2 at $\tau < 0.5$ (Chisholm et al. 2020). The complicating factor in the resonant scattering in the outer Mg II nebula around η Car is that the source of UV photons to be scattered is the Mg II line emission from the dense stellar wind of η Car itself. The spectrum of the central star has a complicated Mg II profile, because each of the two lines has a strong blueshifted P Cygni absorption trough from the wind. While the 2803 \AA line shows a very strong

wind emission component, the emission component of the 2796 Å line is almost completely quashed by the overlapping blueshifted absorption of the 2803 Å line (Cassatella, Giangrande & Viotti 1979; Baratta, Cassatella & Viotti 1995; Hillier et al. 2006), while the wind line profiles are also time variable due to the influence of η Car's hot companion star (Groh et al. 2010, 2012). The much brighter 2803 Å emission from the wind can be seen qualitatively in the pattern of Mg II emission arising from dust-scattered starlight in the Homunculus in Fig. 3(b). In addition, the Mg II emission/absorption that emerges from the dense stellar wind of η Car itself must then pass through the dense walls of the Homunculus nebula, where it suffers additional velocity-dependent absorption (Nielsen, Gull & Vieira Kober 2005). A Mg II atom outside the Homunculus will then ‘see’ an illumination source that is a redshifted version of the complicated stellar spectrum after it passes through the Homunculus. At the rest wavelength of this Mg II atom, there are therefore relatively fewer available 2796 Å photons to scatter, whereas there is an abundance of 2803 Å photons from the strong emission in this line from the central wind. We conclude that this complicated filtering of the stellar spectrum, rather than the density of the outer Mg II atomic gas itself, is primarily responsible for the low observed $\lambda 2796/\lambda 2803$ flux ratio in the outer nebula in both polar directions. It is therefore not straightforward to derive an optical depth and column density from the Mg II doublet ratio in the outer nebula.

5 DISCUSSION

5.1 Age of the Homunculus

The proper motions from Mg II emission for features that are within about 10 arcsec of the star in Fig. 2 display an ejection date of 1847. This material corresponds to the polar lobes of the Homunculus, and the detected light in the $F280N$ filter in the lobes is dominated by scattered starlight (including scattered Mg II emission from the star) rather than resonant scattering of Mg II in the lobes themselves. The 1847 ejection date agrees very well with several previous studies of the expansion of the Homunculus using *HST* imaging (Smith & Gehrz 1998; Morse et al. 2001; Smith 2017). Although not new, this good agreement is actually physically significant in its own right.

Measuring proper motions in *HST*/WFPC2 images from 1995 to 1999 yielded a date of 1847 ± 4 (Morse et al. 2001). Here, we measure precisely the same ejection date with similar precision, but we do so in images with a 2 yr baseline from 2018 to 2020 – over 20 yr later. This 20+ yr timespan is more than 10 per cent of the age of the Homunculus. The fact that we find the same date of origin from the motion at two different epochs provides strong confirmation that the Homunculus nebula is not accelerating or decelerating. In principle, it might accelerate if it is pushed from the inside by a strong post-eruption stellar wind, or might decelerate if it is running into dense material. The lack of any detectable deceleration over time is consistent with the extremely large mass inferred for the Homunculus (Smith et al. 2003a) and the relatively low mass of the Mg II nebula estimated in Paper I.

5.2 3D Kinematics of the Mg II nebula and implications

Paper I proposed that the bulk of the Mg II emission detected in the $F280N$ filter that is seen outside the Homunculus, but inside the N-rich shell of Outer Ejecta, arises predominantly from resonant scattering in the Mg II $\lambda\lambda 2796, 2803$ doublet. Resonant scattering traces warm neutral atomic gas, rather than recombination emission from ionized and cooling post-shock gas.

It has long been recognized that the Outer Ejecta beyond the Homunculus – such as the red S Ridge of material in the lower-right portion of Fig. 1 – appear to arise from one or more older eruptive mass-loss events (Walborn, Blanco & Thackeray 1978; Walborn & Blanco 1988; Morse et al. 2001; Kiminki, Reiter & Smith 2016). Recent proper-motion measurements of the X-ray shell (Corcoran et al. 2022) confirm the general picture that the excitation of the optical knots in the Outer Ejecta arises because slower, older material is being overtaken by fast ejecta from the Great Eruption (Smith & Morse 2004; Smith 2008). Most studies of the Outer Ejecta have concentrated on morphology and kinematics (both proper motions and Doppler shifts) measured from $H\alpha$ and the adjacent [N II] emission lines (Meaburn, Wolstencroft & Walsh 1987). However, it was unclear whether all the ejecta were visible and emitting because dense knots are photoionized by the tremendous Lyman continuum luminosity of the >60 O-type stars in the surrounding Carina Nebula (Smith 2006a), or if we were only seeing a portion of the outflowing ejecta that glows because it has just been shocked by crashing into older ejecta or ambient cloud material.

The Mg II emission distribution is largely anticorrelated with the [N II] + $H\alpha$ structures in the outer nebula beyond the Homunculus lobes in Fig. 1, yet the Mg II ($F280N$) proper motions in the lower panel of Fig. 2 bear a strong resemblance to the [N II] + $H\alpha$ ($F658N$) proper motions in fig. 4 of Morse et al. (2001). The emission distribution, morphology, and kinematics indicate: (1) there is indeed an additional reservoir of ejected material older than the Great Eruption that is not represented in other UV–optical–near-infrared (NIR) emission-line images (Morse et al. 1998; Chesneau et al. 2005; Smith & Morse 2019) or X-ray maps (Seward et al. 2001; Hamaguchi et al. 2018) of shocked-excited gas; (2) the fluffy, filamentary appearance of the extended Mg II features in Fig. 1 – together with a ubiquitous fog of fainter emission surrounding the Homunculus lobes best seen in the black-and-white rendering in Fig. 2 that contrasts sharply with the highly compact and knotty appearance of the [N II] + $H\alpha$ emitting Outer Ejecta – does not seem consistent with having been overrun (i.e. compressed and accelerated) by a fast-moving blast wave generated during the Great Eruption (Smith 2008; Smith et al. 2018b; Corcoran et al. 2022); and (3) because the Mg II nebula represents unshocked ejecta, its kinematics could provide the best indication of the stellar wind history during the decades leading up to the Great Eruption.

Several characteristics of the imaging and spectroscopic observations may be important for determining the geometry of the Mg II-emitting gas. First, the ‘God rays’ (radial shadows) in the near-side Mg II nebulosity trace back to specific dust features on the face of the SE lobe, demonstrating that some of the Mg II-emitting gas fills the volume out in front of the approaching lobe. Secondly, the Mg II emission tends to fill gaps between the dusty lobes and the ionized outer debris, and also within the structures seen in [N II] + $H\alpha$ such as the equatorial NN Jet and channel towards the S Condensation. Thirdly, the NW and SE portions of the nebula show symmetrical radial velocities, but there are no dramatic radial velocity gradients or split line profiles indicating multiple, distinct (optically thin) structures along the line of sight. The exception is the position just outside the edge of the NW lobe, which shows a secondary peak on the redshifted side of both $\lambda 2796$ and $\lambda 2803$ line profiles at approximately $+630 \text{ km s}^{-1}$. (Unfortunately, the ion repeller wire disrupts this portion of the NW spectrum.) And, fourthly, the FWHM emission-line widths are substantially larger than the intrinsic spectral resolution, suggesting that the STIS aperture captures a continuous range of radial velocities through

the outflowing gas, even if brighter knots and filaments within the slit dominate the morphology.

The proper-motion kinematics of the Mg II nebula and the S Ridge observed in [N II] + H α are similar, and these two gas components appear to be part of the same mass-loss phase prior to the Great Eruption but seen through different ionization mechanisms – the Mg II nebula is seen via resonant scattering of near-ultraviolet (NUV) photons from the central star, and the S Ridge (and other Outer Ejecta features) emitting due to shock excitation. Because the range of proper-motion ejection dates for each component is far larger than that measured for the Great Eruption material, it is tempting to infer that the older, outer debris were not ejected in a single eruption but during a sequence of several repeating eruptions or quasi-continuously. We caution that the Mg II proper motions could be improved with a longer time baseline, and the scatter in the proper-motion measurements may be reduced.

The Mg II emission distribution is somewhat diffuse (fog-like) but always inside the outer nebula structures delineated by [N II] + H α , largely tracing the bipolar geometry of the Homunculus, although with distinct filaments that may signify mass-loss variations (see Fig. 1, top panel of Fig. 2, and fig. 1 of Paper I). The STIS slit was placed to cut across some of these filaments, though overall the cross-dispersion Mg II emission is fairly smooth. Combining the main radial velocity component on each side of approximately -340 km s^{-1} to the SE and $+340 \text{ km s}^{-1}$ to the NW with an observed transverse velocity of $\sim 600 \text{ km s}^{-1}$ corresponds to a space velocity $V_S \approx 690 \text{ km s}^{-1}$ and projected motion $\pm 30^\circ$ out of the plane of the sky. The polar axis of the Homunculus lobes is tilted $\sim 41^\circ$ to our line of sight (Smith 2006b), which places the extended Mg II emission roughly 20° away from the polar axis, similar to the half opening angle of the lobes. This suggests that the Mg II filaments in the STIS aperture – which to the NW were described in Paper I as ‘troll hair’ in appearance – lie on a surface (sheet or side walls of a cone). Meanwhile, the faster redshifted Mg II component to the NW would be close to the polar axis. Additional deep Mg II spectra with the STIS long slit oriented perpendicular to the flow direction in the outer NW and SE nebular regions would be highly desirable to further elucidate the large-scale kinematics and constrain the outflow geometry.

The total mass inferred for the Mg II nebula of around $0.02 M_\odot$ (Paper I) is only an order-of-magnitude estimate. But assuming that this material was ejected over a timespan of a few decades before the Great Eruption, as suggested by the scatter in the proper motions, this would imply an average polar mass-loss rate of around $10^{-3} M_\odot \text{ yr}^{-1}$ in the time before the eruption. While we reiterate that this is a very rough estimate, it is consistent with values inferred for the present-day stellar wind of η Car (Smith et al. 2003b; Hillier et al. 2006). It is, however, much lower than the mass-loss rate needed to produce an equatorial torus capable of pinching the waist of the Homunculus. This signals that the pre-eruption mass-loss of η Car was highly asymmetric, with a slow concentrated flow in the equatorial plane, and a lower density, faster wind towards the poles. Perhaps this can be tested if light echoes are discovered that view the pre-eruption star from a poleward direction; if so, we might predict the presence of broad H α emission and P Cygni absorption at -600 to -700 km s^{-1} before the eruption. Light echo spectroscopy viewed from a vantage point near η Car’s equatorial plane has already shown evidence for a slower ($\sim 100 \text{ km s}^{-1}$) equatorial outflow (Smith et al. 2018b).

5.3 Test of Great Eruption models

As noted earlier, Smith et al. (2018b) proposed a model for η Car wherein the Great Eruption resulted from a merger in a hierarchical triple system. These authors proposed that the Outer Ejecta were produced by early grazing collisions of the inner binary, whereas the Homunculus was ejected in the final merger event. In this construct, the bipolar shape of the Homunculus resulted when the merger ejecta collided with a pre-existing dense torus that had been expelled during the inspiral phase in the decades preceding the merger. This torus would have pinched the waist of the bipolar nebula (Frank, Balick & Davidson 1995; Langer, Garcia-Segura & Mac Low 1999; Morris et al. 1999; Smith, Ginsburg & Bally 2018a). Such an interaction between the merger ejecta and the torus may have powered a significant fraction of the luminosity of the Great Eruption (Smith 2013; Smith et al. 2018b). After sweeping through this torus, the bipolar nebula then follows free-expansion, exhibiting a Hubble-like flow in modern proper-motion data.

More recently, Hirai et al. (2021) presented numerical simulations for portions of this merger scenario, and suggested a different explanation for the origin of the bipolar shape of the Homunculus. These authors suggested that the bipolar shape was caused when a prolate super-Eddington wind from the rapidly rotating post-merger star swept into the merger ejecta. These two models make different testable predictions for the kinematics of material immediately outside the Homunculus: namely, in the scenario proposed by Smith et al. (2018b), the material outside the Homunculus was ejected during the inspiral phase in the decades preceding the merger that caused the Great Eruption, whereas in the scenario favoured by Hirai et al. (2021), the material immediately outside the bipolar Homunculus is composed of roughly $10 M_\odot$ of ejecta mass from the merger event, which has yet to be swept up and is a Hubble-like flow that originated in 1843.

The proper motions in Fig. 1 seem initially to contradict the model favoured by Hirai et al. (2021), because this outer material is clearly older than 1843. Instead, the proper motions of Mg II filaments seem more consistent with the model proposed by Smith et al. (2018b), where the gas immediately outside the Homunculus is a few decades older, expelled by the system during the inspiral phase that preceded the merger event. Thus, if the Great Eruption was indeed a stellar merger event, then the Mg II proper motions favour the scenario for shaping the Homunculus proposed by Smith et al. (2018b). In that case, the Mg II nebulosity probably traces ejecta from violent binary interactions during the critical pre-merger inspiral phase, perhaps analogous to the repeating SN impostor eruptions seen in SN 2000ch and AT 2016blu (Aghakhanloo et al. 2023a, b). However, the proper motions themselves do not directly confirm that the 19th century event was indeed a merger. If it was not, then the Mg II nebulosity provides information about the mass-loss and growing instability of the star in the years preceding the Great Eruption, whatever the underlying cause of that eruption may have been.

Doppler shifts that give the orientation (polar or equatorial) and estimates of the optical depth and mass are needed to confidently test any model. So far, Mg II is the only emission line in the UV/optical/IR spectrum that traces the neutral gas that fills the gap between the extended [N II]/X-ray emitting material and the dusty bipolar Homunculus nebula, and so forms the best opportunity to measure the mass-loss properties of the star immediately before the eruption.

6 SUMMARY

We present the first proper-motion measurements made with 2018 and 2020 *HST*/WFC3 UVIS images of η Carinae. These images are taken in the *F280N* filter that samples resonantly scattered emission of Mg II $\lambda\lambda 2796, 2803$ arising from neutral atomic gas that is sandwiched between the outer surface of the dusty Homunculus and inside the ionized [N II]-emitting Outer Ejecta (Smith & Morse 2019). We also present STIS long-slit spectra of the Mg II emission from this nebulosity. So far, Mg II emission appears to be a unique tracer of this material. The main results and implications of this kinematic study are as follows:

(i) Proper motions of material in the polar lobes of the Homunculus (where the *F280N* filter traces dust-scattered starlight) yield an ejection date of 1847, assuming linear motion, in good agreement with previous studies (Morse et al. 2001; Smith 2017). While not surprising, this agreement is physically significant, because deriving the same ejection date from data taken 20+ yr apart confirms that the motion is indeed linear (i.e. not decelerating).

(ii) For the Mg II nebulosity outside the Homunculus, however, *F280N* proper motions neither give a clear single age nor follow a tight Hubble-like flow. Instead, this material is clearly several decades older than the Homunculus, with a range of apparent ejection dates from the late 18th century to the mid-19th century.

(iii) Since the gas in the Mg II nebula is several decades older than the Homunculus, this helps to distinguish between two competing versions of the merger-in-a-triple scenario for η Car's Great Eruption. The measurements contradict expectations of the model proposed by Hirai et al. (2021), where material just outside the Homunculus is high-mass merger ejecta, and where the bipolar structure of the Homunculus arises when the merger ejecta are shaped by a post-eruption bipolar super-Eddington wind from a rapidly rotating merger product. Instead, the presence of older pre-eruption wind material just outside the Homunculus lobes favours a model proposed by Smith et al. (2018b) in which the waist of the merger ejecta is pinched by a torus ejected during the pre-merger inspiral phase.

(iv) The observed line ratio Mg II $\lambda 2796/\lambda 2803 < 0.5$ across the nebulosity sampled by the STIS long-slit spectrum is unusually low, even for an optical depth of $\tau \sim 1$. Because the line ratios are similar in the bipolar directions and the kinematics are well offset from ISM or other absorption components along our line of sight, we conclude that the low $\lambda 2796/\lambda 2803$ line ratio in the extended nebulosity is due to the intrinsic P Cygni Mg II profile, preferentially attenuating the bluer $\lambda 2796$ line, which forms the source of the resonantly scattered UV photons from the central star.

(v) Proper motions give tangential expansion speeds of around 600 km s^{-1} , whereas radial velocities of the Mg II emission are $\pm 340 \text{ km s}^{-1}$. This, combined with the relatively narrow velocity dispersion of the Mg II emission, suggests that much of it arises in the walls of a cone with an opening angle of about 20° from the polar axis, with radial expansion speeds of around 700 km s^{-1} . We caution, however, that the extended Mg II emission in STIS spectra is detected at low signal-to-noise ratio, so that we are only detecting the brightest of the Mg II features seen in images. Our understanding of the structure and kinematics of the Mg II nebula would be significantly improved with deeper long-slit spectra.

(vi) Combining the ejection dates inferred from kinematics of the Mg II nebulosity with a very rough mass estimate for the Mg II nebula from Paper I, we find that the implied average mass-loss rate needed to create the Mg II nebula is comparable to the current mass-loss rate of the central star. We therefore conjecture that the pre-eruption system may have had a fast polar wind similar to its present-day

wind (Smith et al. 2003b), which is in stark contrast to the dense equatorial outflow that would have been needed to pinch the waist of the Homunculus. So far, the Mg II nebula is the only way to study this pre-eruption polar wind from η Car, although this may change if light echoes are discovered that view the pre-eruption star from the polar direction. We noted predictions of what might be seen in this case.

ACKNOWLEDGEMENTS

This study is based on observations made with the NASA/ESA *Hubble Space Telescope*, obtained at the Space Telescope Science Institute (STScI), operated by the Association of Universities for Research in Astronomy, Inc., under NASA contract NAS 5-26555. The authors appreciate the assistance of STScI staff, especially Dr. Amber Armstrong, in planning and executing the WFC3 and STIS observations. Support was provided by NASA through grants GO-15823, GO-15596, GO-15289, GO-14768, and AR-14586 from STScI. NS's research on η Carinae also received support from NSF grants AST-1312221 and AST-1515559.

DATA AVAILABILITY

The data underlying this article are publicly available in the Mikulski Archive for Space Telescopes (*MAST*) at the Space Telescope Science Institute at <https://mast.stsci.edu/search/ui/#/hst> under proposal IDs 15289 and 15823.

REFERENCES

- Aghakhanloo M. et al., 2023a, *MNRAS*, 521, 1941
Aghakhanloo M. et al., 2023b, *MNRAS*, 526, 456
Baratta G. B., Cassatella A., Viotti R., 1995, *A&AS*, 113, 1
Cassatella A., Giangrande A., Viotti R., 1979, *A&A*, 71, L9
Chesneau O. et al., 2005, *A&A*, 435, 1043
Chisholm J., Prochaska J. X., Schaerer D., Gazagnes S., Henry A., 2020, *MNRAS*, 498, 2554
Corcoran M. J. et al., 2022, *ApJ*, 937, 122
Currie D. G. et al., 1996, *AJ*, 112, 1115
Currie D. G., Dorland B. N., Kaufer A., 2002, *A&A*, 389, L65
Davidson K., Humphreys R. M., 1997, *ARA&A*, 35, 1
Davidson K. et al., 1986, *ApJ*, 305, 867
Frank A., Balick B., Davidson K., 1995, *ApJ*, 441, L77
Gaviola E., 1950, *ApJ*, 111, 408
Groh J. H., Madura T. I., Owocki S. P., Hillier D. J., Weigelt G., 2010, *ApJ*, 716, L223
Groh J. H., Hillier D. J., Madura T. I., Weigelt G., 2012, *MNRAS*, 423, 1623
Hamaguchi K. et al., 2018, *Nat. Astron.*, 2, 731
Hillier D. J. et al., 2006, *ApJ*, 642, 1098
Hirai R. et al., 2021, *MNRAS*, 503, 4276
Kiminki M., Smith N., 2018, *MNRAS*, 477, 2068
Kiminki M., Reiter M., Smith N., 2016, *MNRAS*, 463, 845
Langer N., Garcia-Segura G., Mac Low M. M., 1999, *ApJ*, 520, L49
Leutenegger M. A., Kahn S. M., Ramsay G., 2003, *ApJ*, 585, 1015
Meaburn J., Wolstencroft R. D., Walsh J. R., 1987, *A&A*, 181, 333
Mehner A. et al., 2016, *A&A*, 595, 120
Morris P. W. et al., 1999, *Nature*, 402, 502
Morse J. A., Davidson K., Bally J., Ebbets D., Balick B., Frank A., 1998, *AJ*, 116, 2443
Morse J. A., Kellogg J. R., Bally J., Davidson K., Balick B., Ebbets D., 2001, *ApJ*, 548, L207
Nielsen K. E., Gull T. R., Vieira Kober G., 2005, *ApJS*, 157, 138
Owocki S. et al., 2004, *ApJ*, 616, 525
Prieto J. L. et al., 2014, *ApJ*, 787, L8

- Quataert E., Fernández R., Kasen D., Klion H., Paxton B., 2016, *MNRAS*, 458, 1214
- Rest A. et al., 2012, *Nature*, 482, 375
- Seward F. D. et al., 2001, *ApJ*, 553, 832
- Shaviv N. J., 1998, *ApJ*, 494, L193
- Shull J. M., Darling J., Danforth C. W., 2021, *ApJ*, 914, 18
- Smith N., 2002, *MNRAS*, 337, 1252
- Smith N., 2006a, *MNRAS*, 367, 763
- Smith N., 2006b, *MNRAS*, 644, 1151
- Smith N., 2008, *Nature*, 455, 201
- Smith N., 2013, *MNRAS*, 429, 2366
- Smith N., 2014, *ARA&A*, 52, 487
- Smith N., 2017, *MNRAS*, 471, 4465
- Smith N., Frew D., 2011, *MNRAS*, 415, 2009
- Smith N., Gehrz R. D., 1998, *AJ*, 116, 823
- Smith N., Morse J. A., 2004, *ApJ*, 605, 854
- Smith N., Morse J. A., 2019, *MNRAS*, 489, 268 (Paper I)
- Smith N., Owocki S. P., 2006, *ApJ*, 645, L45
- Smith N., Gehrz R. D., Hinz P. M., Hoffmann W. F., Hora J. L., Mamajek E. E., Meyer M. R., 2003a, *AJ*, 125, 1458
- Smith N., Davidson K., Gull T. R., Ishibashi K., Hillier D. J., 2003b, *ApJ*, 586, 432
- Smith N., Ginsburg A., Bally J., 2018a, *MNRAS*, 474, 4988
- Smith N. et al., 2018b, *MNRAS*, 480, 1457
- Smith N. et al., 2018c, *MNRAS*, 480, 1466
- Thackeray A. D., 1950, *MNRAS*, 110, 524
- Walborn N. R., 1976, *ApJ*, 204, L17
- Walborn N. R., Blanco B., 1988, *PASP*, 100, 797
- Walborn N. R., Blanco B. M., Thackeray A. D., 1978, *ApJ*, 219, 498

This paper has been typeset from a $\text{\TeX}/\text{\LaTeX}$ file prepared by the author.